8-2016

Deceleration of droplets that glide along the free surface of a bath

Jacob Hale
DePauw University, jacobhale@depauw.edu

Caleb Akers
DePauw University, calebakers_2017@depauw.edu

Recommended Citation

Accepted manuscript of an article published in *Journal of Fluid Mechanics* (2016), vol. 803, pp. 313-331 DOI: http://dx.doi.org/10.1017/jfm.2016.481

Deceleration of droplets that glide along the free surface of a bath

Jacob Hale[1]† and Caleb Akers[1]

[1]Department of Physics and Astronomy, DePauw University, Greencastle, IN 46135, USA

(Received xx; revised xx; accepted xx)

(**Published in The Journal of Fluid Mechanics (2016), *vol.* 803, *pp.* 313-331**)

A droplet obliquely impacting a bath surface of the same fluid can traverse along the interface while slowing at an exponential rate. The droplet rests on a thin film of air and deforms the bath surface creating a dimple and travels along the surface similar to a wave pulse. Viscous coupling of the droplet and bath surfaces through the air film leads to viscous drag on the bath and perturbs the wave motion of the otherwise free surface. Even though Reynolds numbers are greater than unity ($Re\,O(10-100)$), we show that the droplet's deceleration is only due to viscous coupling through the air gap. The rate of deceleration is found to increase linearly with droplet diameter.

1. Introduction

The phenomenon of a liquid droplet resting on the surface of a bath of the same fluid was first described over a hundred years ago (Reynolds 1881) and continues to interest scientists and the public because of many remaining questions about the process (Walker 1978). The literature has established the intervening air layer model to explain noncoalescence of miscible fluids in contact (see review by Neitzel & Dell'Aversana (2002)). A millimeter-sized droplet of water gently deposited onto the surface of an unperturbed bath of water will undergo coalescence within a few tens of milliseconds (Thoroddsen & Takehara 2000). Coalescence can be delayed for approximately one second with the addition of surfactants (Amarouchene *et al.* 2001), and when the intervening fluid has a large density, coalescence can be delayed for > 10 seconds (Charles & Mason 1960*a*).

Rupture occurs once the air gap thickness is $O(10^{-7})$ m, within the range of van der Waals forces (Hahn *et al.* 1985). Rupture of the air gap can result in a repetition of partial coalescence, termed the coalescence cascade (Charles & Mason 1960*b*). The time scale of coalescence (Thoroddsen & Takehara 2000) and the bouncing of the daughter droplets (Honey & Kavehpour 2006) have been reported in past studies.

Coalescence of miscible fluids can be delayed, even indefinitely, by replenishing the air layer. One such method uses a thermal gradient across the air gap causing air entrainment in the gap by Marangoni convection of the liquids (Dell'Aversana *et al.* 1996). A more popular method can sustain a droplet by oscillating the bath so as to lift the droplet from the bath once each cycle (Couder *et al.* 2005). This has led to a number of interesting observations concerning how the droplet interacts with the waves it generates upon impact, including relevant quantum physics analogs (Couder & Fort 2006),(Fort *et al.* 2010),(Andersen *et al.* 2015).

Forcing the droplet or bath into relative, tangential motion with respect to the other can also drive air into the gap so as to develop sufficient lubrication forces to levitate the

† Email address for correspondence: jacobhale@depauw.edu

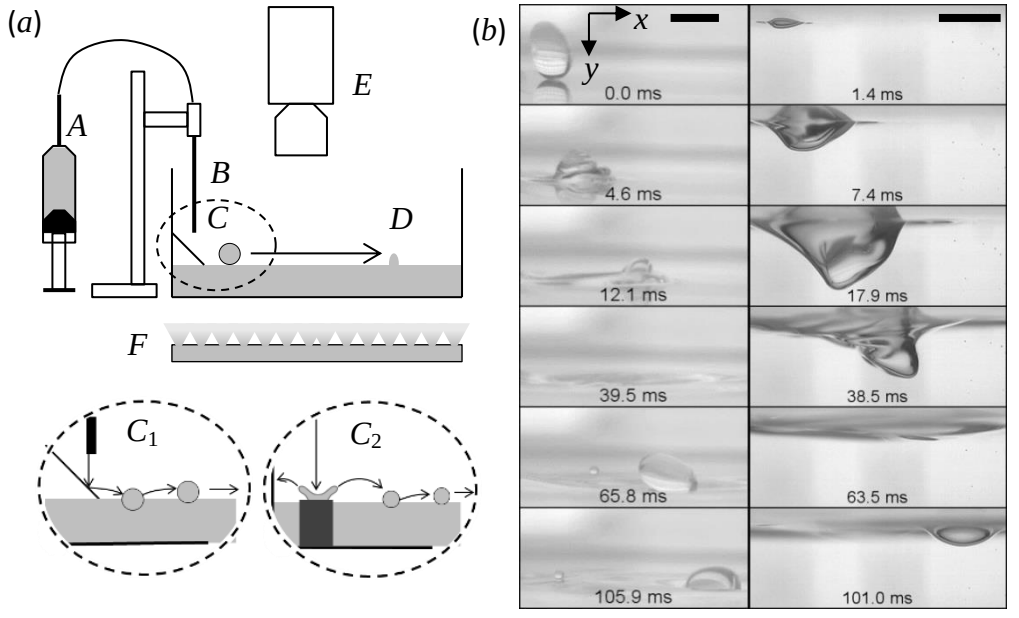

FIGURE 1. Experimental setup. (a) A syringe pump (A), pushes fluid through an interchangeable stainless steel nozzle (B). Released droplets fall onto a bath (C) and decelerate until coalescence (D). A high-speed camera (E) collects images from above with diffused lighting below (F). (C_1) Larger droplets rebound from an incline, impact the bath and stabilize. (C_2) In an alternate configuration, high-speed droplets impact an aluminum block making a splash, daughter droplets then impact the bath, and stabilize. (b) Image sequence of a droplet impacting the bath. Side views from above (left) and below (right) the surface (cameras are not synchronized; maximum error in relative times is 0.55 ms); $We_x = 24.1$, $We_y = 36.6$. Scale bars are 4 mm.

droplet. This has been achieved by holding a droplet above but in contact with a rotating bath (Dell'Aversana *et al.* 1996), placing a droplet inside a horizontally rotating cylinder coated with a film of the same fluid (Lhuissier *et al.* 2013), or capturing a droplet on the edge of a hydraulic jump (Sreenivas *et al.* 1999), (Pirat *et al.* 2010). In these cases the system is in steady state. As long as the driving force is maintained, the coalescence of the droplet can be inhibited.

What happens to the droplet if the driving force were subsequently turned off? In this report we answer this question by presenting experiments on the transient dynamics of a droplet that moves, or skirts, across the free surface of a bath of the same fluid in the absence of any driving force. This work builds on observations of the phenomenon which have been reported since the late 1800s (Reynolds 1881), (Cai 1989), (Klyuzhin *et al.* 2010), (Alghoul *et al.* 2011). We use high-speed imaging to record the center of mass motion and internal flow of the droplet along with the internal flow of the bath. The droplet velocity is observed to decrease exponentially. Herein, the only parameter we explore is droplet diameter. Though the interactions with the droplet and the free surface are complex, the observed motion can be explained with a simple model of a modified Stokes drag.

2. Experimental Methods

2.1. *Droplet generation*

In the experimental setup shown in figure 1 a syringe delivers fluid to an interchangeable stainless steel nozzle fixed to a vertical translation stage. Single droplets with diameters greater than 1.5 mm fall from the nozzle and impact a clean glass microscope slide inclined at 45° (Figure 1*a*). A few droplets are released to wet the slide. A single droplet is then released and, rebounding from the wetted incline, falls on the surface of the bath with a velocity component tangent to the surface (Figure 1*b*), where it decelerates along the surface until coalescence. Smaller droplets ($D < 1.5$ mm) are created from the secondary products of higher velocity droplets falling onto a shallow pool as illustrated in figure 1*a*. In this case the height of the nozzle is increased to > 20 cm and the falling droplet impacts a thin film atop an aluminum block, the upper horizontal surface of which slightly protrudes from the free surface of the bath. A splash results and daughter droplets of various sizes are ejected from the splash crown at low angles so as to impact the bath surface with a large tangential velocity component. Droplets observed from a bottom-up or a top-down view had diameters between $0.77 \leqslant D \leqslant 3.87$ mm. Smaller droplets ($D < 1.5$ mm) could not be imaged from side views because their motion was not confined to the focal plane of the camera. Droplets larger than 1.5 mm were therefore used in experiments that required imaging from the side to provide a consistent breadth in the range of droplet diameters ($1.51 \leqslant D \leqslant 4.67$ mm) for all views.

Reverse osmosis water is used with the addition of the non-ionic surfactant Triton X-100 which has a critical micellar concentration (cmc) of 0.5 g/L. The surfactant enhances the survival of droplets during impact (Amarouchene *et al.* 2001) and stabilizes the free surface (Gatne *et al.* 2009). Further, it increases the surface viscosity with air and thus increases the coupling of the interface between the droplet and the bath (Amarouchene *et al.* 2001). All experiments quantitatively discussed here and shown in the figures used 0.3 cmc surfactant solution, though additional experiments using pure water or silicone oils were performed for qualitative comparisons. The surface tension (σ) and kinematic viscosity (ν) of the aqueous surfactant solution were measured to be 0.0316 ± 0.0002 N/m and 1.023 ± 0.030 cst respectively. The same fluid is used for both the bath and the droplets in each trial and both are maintained at the same temperature (20° C) for all experiments.

The bath is kept in a 100 x 300 mm glass tank that is filled to a depth of 25 mm and can be considered the deep pool limit. Viscous effects due to the rigid container are therefore considered negligible. Waves created by the impact dissipate before reflections from the container walls can occur. Some small amplitude waves originating from the impact did reach the site of the moving droplet after reflecting from the container walls. However, we did not observe any systematic effect from these waves on the motion or coalescence of the droplet. We should note that Dell'Aversana *et al.* (1996) observed a wake in the bath behind a pendant drop that was held above and in contact with a rotating bath. In this work no wake is observed. The Reynolds number for that system ($Re = uD/\nu$) is double the largest values for droplets in this work when the diameter of the droplet rather than the droplet radius is used for the length scale, as it is here. Further, it is unclear if the shallow container used by Dell'Aversana *et al.* (1996) for the bath was sufficiently deep to decouple the rigid container walls from the free surface flow. Finally, though the pendant droplet was observed to rotate in that work, it was in strong contact with a rigid post which would significantly dampen the flow rate in the droplet and thus likely cause a greater velocity gradient between the droplet and the bath than what is observed here for the freely gliding droplets.

2.2. *High-speed imaging system*

A high-speed camera recorded the droplet motion with diffuse, backlit illumination provided by a bank of LED lights. The transparent tank allowed the camera to be positioned to record from above (as seen in figure 1*a(E)*), from below or from the side. Trajectories ($x(t)$) were recorded from a top-down view whereas side views and bottom-up views were used to record the internal motion of the droplet and bath as well as to determine droplet and interface geometries. Glass bubbles (diameter $< 50\,\mu$m, 0.11 g/ml, Pro Marine Supplies), commonly used as a light-weight epoxy filler for marine applications, were used in the bath to monitor the motion of the bath surface. The glass bubbles are less dense than water so as to float, marking the fluid motion at the bath surface. Neutral density polystyrene beads ($53 - 63\,\mu$m, Cospheric) were added to the droplets when imaging the rotational motion. The markers were imaged from both below and from the side. Images were recorded with a Miro 310 monochrome camera (Vision Research) equipped with a 105 mm macro lens. For some experiments a second, simultaneous view was obtained by using a Hotshot 512SC (NAC). Though not synchronized, maximum error in relative times was not significant. When simultaneous images are presented the maximum relative error is given. The smallest features (e.g., droplet rupture) were recorded at an optical resolution of 7.8 μm, whereas the largest features (e.g., droplet trajectories) were recorded at an optical resolution 101 μm. Droplet impact and rupture were recorded at 8000 frames per second (fps). All other data was recorded at 2000 fps.

2.3. *Experimental variables*

In figure 2 we define many of the variables discussed in this work. In addition to these, there are three different time scales: time relative to the moment of impact, t_I, time relative to the onset of skirting motion, t_s, and time relative to rupture, t_r. Other variables will be introduced in context.

The only parameters changed are droplet size and impact velocity, though the latter did not affect the dynamics of skirting. Though impact velocity is surely an important parameter contributing to the probability of droplet survival during impact, the exponential deceleration that follows impact and the conclusions presented in this report are not affected by the dynamics of impact. It was observed that different impact heights and impact angles do lead to a range of speeds at the onset of skirting, which in turn can lead to larger distances traveled. This spread in initial skirting speeds did not affect the dynamics of skirting motion, a result suggested by the self-similarity of exponential decay. The rate of decay is a constant of the motion. We found no significant changes to the results after truncating trajectories and repeating the analysis. Other parameters that are expected to be important to this problem include the surface elasticity (Amarouchene *et al.* 2001) and viscosity. It was not feasible to explore these two parameters but their effect on droplet skirting will be the subject of a future report. Therefore, the only experimental parameter explored in this work is the droplet diameter. We varied D as described above.

3. Results and Discussion

3.1. *Droplet impact*

Both the droplet and the free surface of the bath deform significantly upon impact of the droplet as seen in figure 1*b* (see also Movie 1 in the online supplemental materials). Weber numbers at impact are in the range 5 - 50 ($We = \rho u^2 D/\sigma$), which is the regime of

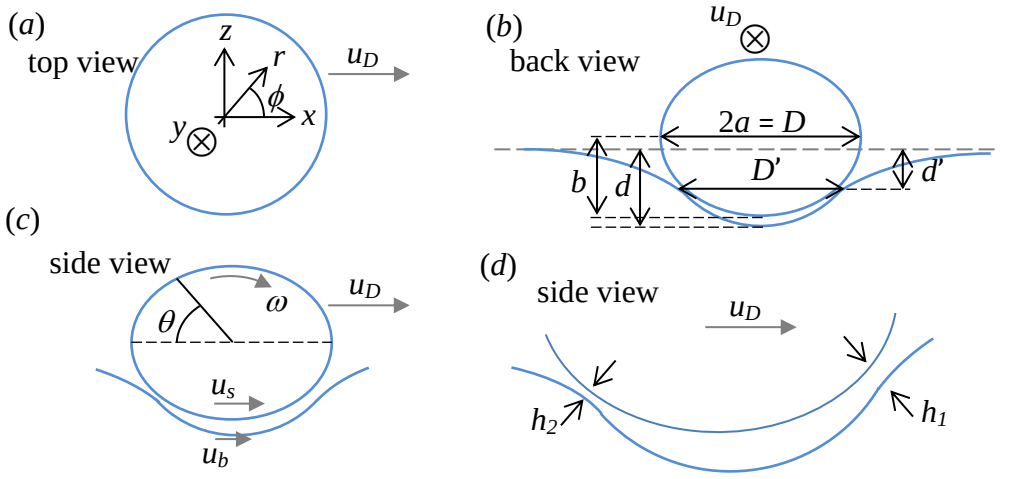

FIGURE 2. Variables defined. (a) Top view diagram of a skirting droplet moving with center-of-mass speed, u_D, in the x-direction. y is measured down from the free surface with z in the plane of motion, transverse to u_D. r is measured radially from the vertical axis of symmetry of the droplet. (b) Back view of the droplet. The droplet diameter, D is measured as twice the semi-major axis, a, of the droplet. The droplet is separated from the bath by an air gap that is bound by a horizontal circle with diameter D'. The depth from the free surface to this plane is d' while the depth of the dimple in the bath is d. b is the semi-minor axis of the lower half of the droplet. (c) Side view diagram. The droplet rolls with slipping with an angular speed ω. The flow inside the droplet just above the air gap has a forward speed u_s relative to the stationary lab frame. The flow inside the bath just below the air gap has a forward speed u_b. (d) The air gap has thickness $h(\theta, \phi)$ with values h_1 and h_2 at the leading and trailing edge of the air gap, respectively.

coalescence for vertically impacting droplets (Hsiao *et al.* 1988) yet the droplets here do not coalesce. The addition of surfactant increases the surface energy of the droplet and bath creating a larger barrier to coalescence (Amarouchene *et al.* 2001), though droplets of pure water also survived impact in our study, albeit less frequently and with less predictable motion. Using pure water for both droplets and the bath Ching *et al.* (1984) shot streams of droplets ($D < 1.2$ mm) at a bath at oblique impact angles ($< 15°$). At similar Weber numbers they found that the first droplet always coalesced at impact and only subsequent droplets in the stream survived impact. In contrast the impact angles here are near 45° from horizontal.

After impact ($t_I = 0$ ms) the droplet oscillates between oblate and prolate shapes along the direction of motion shown in figure 3a and Movie 2. These oscillations decay until the droplet is nearly circular in the horizontal plane (figure 3, $t_I > 150$ ms). The variation in the frame-by-frame measurement of the major axis is large during this oscillatory period but quickly approaches a stable value which is maintained for the remainder of the motion (figure 3b). The stable droplets are slightly oblate along the vertical axis with Bond numbers near unity ($Bo = \rho g D^2/\sigma \approx 1$) and remain so during the rest of the motion (figure 4a). The oblate droplets have a different ellipticity between the top and bottom halves because the bottom is supported by the buoyant force from the displaced fluid in the bath (Ooi *et al.* 2015).

After the transient oscillations have died out the droplet continues forward monotonically, decelerating until eventual coalescence as seen in figure 4b and supplemental Movie 3. We will refer to this long-time motion as skirting ($t_I > 200$ ms for the droplet in

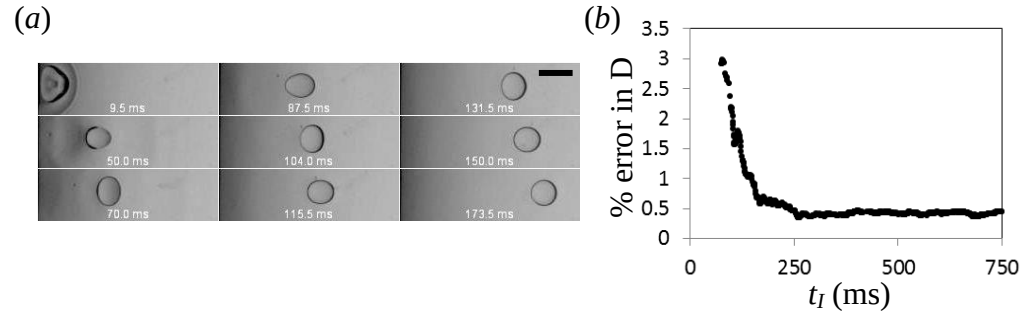

FIGURE 3. Initial droplet oscillations. (a) Top view of initial impact and oscillations of a droplet. Time is measured from the moment of impact, t_I. Scale bar is 4 mm. (b) The standard deviation in the diameter of the droplet for a 25 ms-wide sliding window.

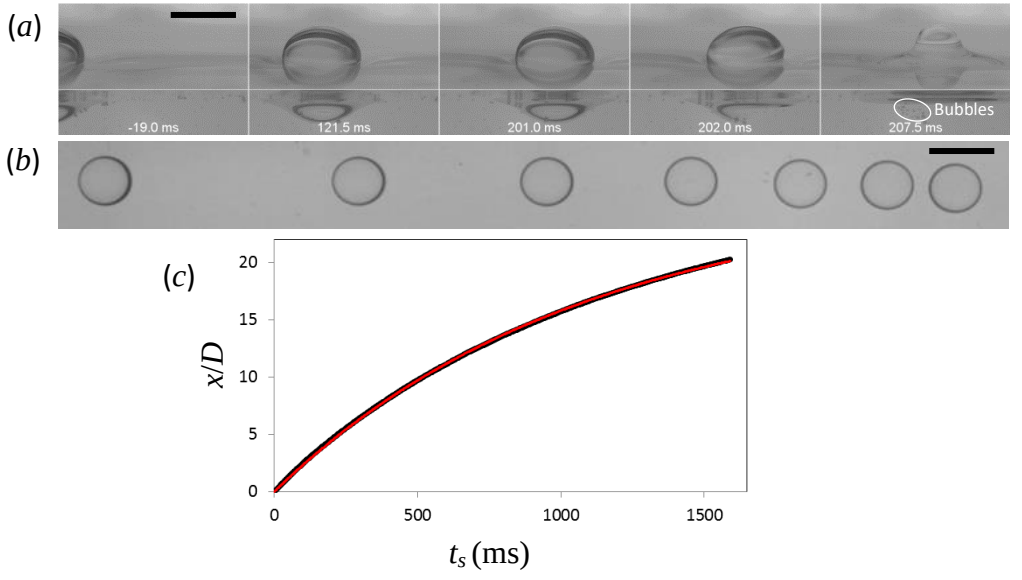

FIGURE 4. Decelerating droplet. (a) Side views of a skirting droplet seen from just above (top) and below (bottom) the free surface. Time is measured from the onset of skirting, t_s. Scale bar is 4 mm. Views are not synchronized; maximum error in relative times less than 0.2 ms. (b) Overlaid image sequence of a long lifetime skirting droplet (different than the droplet in a). Time interval between exposures is $\Delta t = 125$ ms with the first image at $t_s = 0.0$ ms. Scale bar is 4 mm. (c) Position versus time, $x(t)$ for the droplet, data is black and the thin line is a fit to $x(t) = u_0\tau(1 - e^{-t/\tau})$ with $\tau \propto D$. The width of the line represents the measurement error.

figure 3) and define t_s as the skirting time with $t_s = 0$ set to the time when the standard deviation in the diameter of the droplet for a 25 ms sliding window first drops below 0.5%. This occurs at approximately 150 ms after impact for the droplet of figure 3b. The oscillations cause significant and changing inertial interactions with the bath but for $t_s > 0$ the speed of the droplet is small with Capillary numbers much less than 1 ($\mathrm{Ca} = \mu u/\sigma \approx 10^{-3}$). Therefore, the droplet is in a quasi-steady state and thus the geometry of the droplet and dimple resemble that of a stationary droplet (figure 4a, second image pair).

3.2. *Droplet and bath geometry*

As the droplet moves across the free surface it rides in a dimple made by the weight of the droplet (figure 4a). The shape of the dimple is determined by the Young-Laplace relationship. For the bath surface outside the air gap region (bounded by a circle of diameter D' in figure 2*b*) and for the axial symmetry of the problem here, this relationship is given by

$$\rho g y = -\sigma \left[\frac{y_{rr}}{\left(1 + y_r^2\right)^{3/2}} + \frac{y_r}{r\left(1 + y_r^2\right)^{1/2}} \right], \tag{3.1}$$

where y_r is the derivative of surface depth with respect to r measured radially outward from the vertical axis of symmetry. ρ is the density of the fluid, which is the same for both the droplet and the bath (the density of air is negligible), and g is the acceleration of gravity. The surface tension σ of the air-fluid interface is assumed constant for the entire surface of the droplet, assuming a perfectly hydrophobic case due to the continuous air gap separating the droplet from the bath (Mahadevan & Pomeau 1999). The boundary conditions are that $y(r) = 0$ for $r \to \infty$ and at $r = D'/2$ the vertical component of the surface tension force is equal to the weight of the fluid displaced by the meniscus outside of the air gap (Keller 1998). D' is measured to the inflection point in the curvature of the dimple (figure 2*a*). The droplet interacts with the bath through the viscous coupling through the air gap (Couder *et al.* 2005) & (Lhuissier *et al.* 2013). The shape of the dimple bounding the air gap from below closely follows that of the droplet (Couder *et al.* 2005).

It is important to determine the magnitude of the bounding area of the air gap, A_g, between the droplet and the bath since it defines the area of interaction between the two fluid bodies. A quick assumption is that the air gap area would grow as D^2, but the deformability of the two fluid volumes requires that the air gap area scales more like D^3. This is shown in figures 2 and 5. As the Bond number increases, the droplet sinks deeper into the bath (d scales with D) and flattens (figure 2*b*). The air gap diameter D' increases with D but has a slope of unity and thus the fraction of the droplet surface area bounding the air gap increases (figure 5*a*). The air gap area is an elliptical arc of revolution and can be calculated from the surface area integral (derived in the online supplementary materials),

$$\begin{aligned} A_g = \pi a^2 &- \frac{\pi}{a^2}\sqrt{(a^2 - z^2)(a^2 - \epsilon^2 z^2)} \\ &+ \pi a^2 \left(\frac{1 - \epsilon^2}{\epsilon}\right) \ln \left| \frac{a(1+\epsilon)}{\epsilon\sqrt{a^2 - z^2} + \sqrt{a^2 - \epsilon^2 z^2}} \right|, \end{aligned} \tag{3.2}$$

which, for $z = a = D/2$, reduces to the familiar form for the surface area of a hemi-ellipsoid,

$$A_g = \pi a^2 \left[1 + \left(\frac{1 - \epsilon^2}{\epsilon}\right) \tanh^{-1}\epsilon \right]. \tag{3.3}$$

$\epsilon^2 = 1 - (b/a)^2$ is the ellipticity of the bottom half of the droplet. The experimental results confirm that the air gap area scales closer to D^3 (figure 5*b*).

3.3. *Dynamics of the air gap*

Evidence for the air gap is seen by the presence of bubbles that appear during rupture. This can be seen in the last frame of figure 4*a* and figures 6*a* and *b* (see also supplemental Movie 4). The formation of these bubbles is due to Mesler entrainment (Esmailizadeh & Mesler 1986) and is mainly discussed in the literature for the case of a falling droplet that

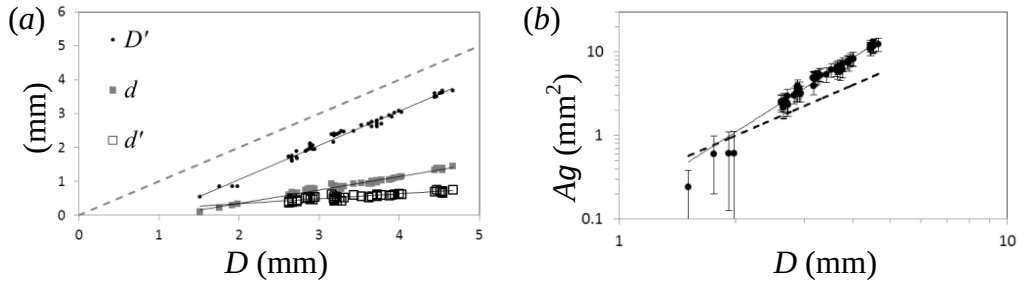

FIGURE 5. Resting geometry of the droplet. (a) D', d' and d each scale linearly with droplet diameter, D. The dashed line has a slope of unity as does D', whereas d and d' have smaller slopes and converge for $D < 2$ mm. (b) Air gap area below the droplet grows as $A_g \propto D^{(2.87\pm0.15)}$, stronger than D^2 (dashed line) owing to both greater submersion and flattening of the droplet.

impacts a deep bath with a low Weber number (Saylor & Bounds 2012) & (Tran *et al.* 2013). These bubbles form when air becomes trapped below the impacting droplet and rupture occurs along the periphery of the air gap (Hendrix *et al.* 2016). As the air film quickly recedes from the first point of rupture, instabilities in the edge of the film cause bubble pinch-off. This leads to a large number of small bubbles beneath the free surface. For the case of skirting droplets reported here, the droplets are not vertically impacting the surface at the time of rupture. The air gap results from air entrainment in the air gap caused by rotational motion of the droplet. A full determination of the gap profile and its thinning behavior can be made using interferometric techniques (Tran *et al.* 2013). Though such an experiment was not feasible in our lab, we analyzed the bubbles created during droplet rupture and present a semi-quantitative description of the geometry and dynamics of the air gap.

The average thickness of the air gap can be estimated by measuring the volume of the air bubbles, Ω_B, resulting from the breakup of the unstable, receding film (Tran *et al.* 2013), (Aryafar & Kavehpour 2008). The volume is found to increase as $D^{(4.3\pm0.4)}$, as shown in figure 6c. Having already shown that the curved surfaces that bound the air gap scale as D^3, the ratio Ω_B/A_g, shows that the average gap thickness, $\bar{h}$, should scale linearly with D. The average thickness at rupture for all droplets is $O(10^{-7} - 10^{-6})$ which is consistent with other work on resting droplets (Couder *et al.* 2005) and is nearly within the range of van der Waals forces.

For vertically impacting drops the excess pressure deforms both the bath and droplet, causing a downward dimple in the bath and an upward dimple in the droplet (Tran *et al.* 2013) & (Bouwhuis *et al.* 2012). The thickness of the gap decreases quickly with time but remains thicker at the vertical axis of the droplet than at the edge of the gap (Tran *et al.* 2013). For the case of a droplet forced into relative motion tangential to and in contact with the free surface of the bath, the gap is thinnest along the sides and back edges of the gap (Lhuissier *et al.* 2013). Such a profile is required by lubrication theory to explain levitation of the droplet (see also Dell'Aversana *et al.* (1996)). Though the skirting motion of the droplets in this report is unlike prior studies, the air gap was also found to be thinner along the periphery. This was determined by measuring the point where rupture began (Charles & Mason 1960a). Invariably, rupture began along the edge of the gap area as is seen in figures 6b & 7 and bridging of the two fluid volumes proceeds fastest along the rim (figure 6b, frames 0.75 and 1.25 ms). Further, for a large majority of cases, rupture began at the sides transverse to the direction of motion ($z = \pm D/2$) and more specifically, for 73.3% of trials (44/60) rupture began at an angular distance

between $\pi/2 - 2\pi/3$ to either side of the forward direction ($\theta = 0$, figure 7). A significant number of rupture points occurred along the trailing edge (13.3%), whereas only 1.6% (only one event in 60 trials) occurred in the front third of the gap periphery.

If we assume that rupture begins at the thinnest point in the film (Charles & Mason 1960*a*) we find that, statistically, the back half of the periphery of the gap is thinner than the front half and that the periphery is everywhere thinner than the rest of the air gap, similar to the gap profile of a droplet held above a moving wall found by Lhuissier *et al.* (2013) using interferometry. As was shown in that work, the constriction on the periphery of the air gap results in a lubrication force that delays coalescence. Although an accurate value of the lubrication force in the case of skirting droplets requires a detailed measurement of the air gap profile (interferometry), we can estimate the force by approximating the gap geometry to be an inclined plate moving near a rigid flat plate. We discuss this approximation in the next section.

Finally, one may wonder whether the air gap gets thinner in time, as is the case for resting droplets. To answer this question we look at rupture as a function of skirting time. For droplets of the same diameter and the same initial conditions, the total bubble volume measured at rupture is seen to be similar over a wide range of droplet lifetimes (see figure 6*c*). Since the air gap area also remains constant during the skirting motion, these results suggest that the average air gap thickness remains the same throughout the motion. This assumes the controlled initial conditions result in the same initial air gap thickness. A full measurement of the air gap profile would be required to check the validity of this assumption. Indeed, it is known that experiments with water droplets are less repeatable than similar experiments with silicone oils and other fluids (Saylor & Bounds 2012). Adding surfactant increases the probability of droplet survival upon impact with a bath (Amarouchene *et al.* 2001) but the spread in droplet lifetimes, T_s, is large (Amarouchene *et al.* 2001), (Mills *et al.* 2011). Despite strict control of initial conditions, including holding the diameter constant, skirting droplets of surfactant laden water also have a large range in lifetimes (see figure 8). The lack of repeatability is often attributed to contaminants in the fluid (Mills *et al.* 2011) that puncture the air gap and not because of variability of controlled initial conditions. Delayed coalescence and maintenance of the air gap requires a driving force, the origin of which is discussed in the next section.

3.4. *Droplet and bath dynamics*

After the transient, oscillatory motion has died out the droplets will skirt along the surface of the bath, slowing exponentially. This is visualized in figure 4*b* where the droplet travels sequentially shorter distances in equal time steps. The forward motion of the center-of-mass of the droplet is shown in figure 4*c*. The motion can be described by an exponential decay function represented by the red line. This function results from a simple model of linear resistance, which is described in Section 3.5.

The droplets can be observed to rotate in a rolling manner throughout the motion by following tracer particles inside the droplets. The onset of rotation occurs very soon after impact and well before $t_s = 0$. Figure 9*a* shows a top-down view of a droplet from impact until soon after the oscillations have died out (see also Movie 5). A tracer particle located just under the surface of the droplet is observed to move forward ahead of the center-of-mass of the droplet, indicating rotation. The position x (fixed lab frame) of the center-of-mass of the droplet and the tracer particle is plotted as a function of time after impact (t_I) in figure 9*b*. The tracer moves with the same forward speed of the droplet at the trailing edge ($\theta = 0$), and nearly double the center-of-mass speed u_D at $\theta = \pi/2$. The motion of the tracer is similar to what we would expect for a sphere rolling with

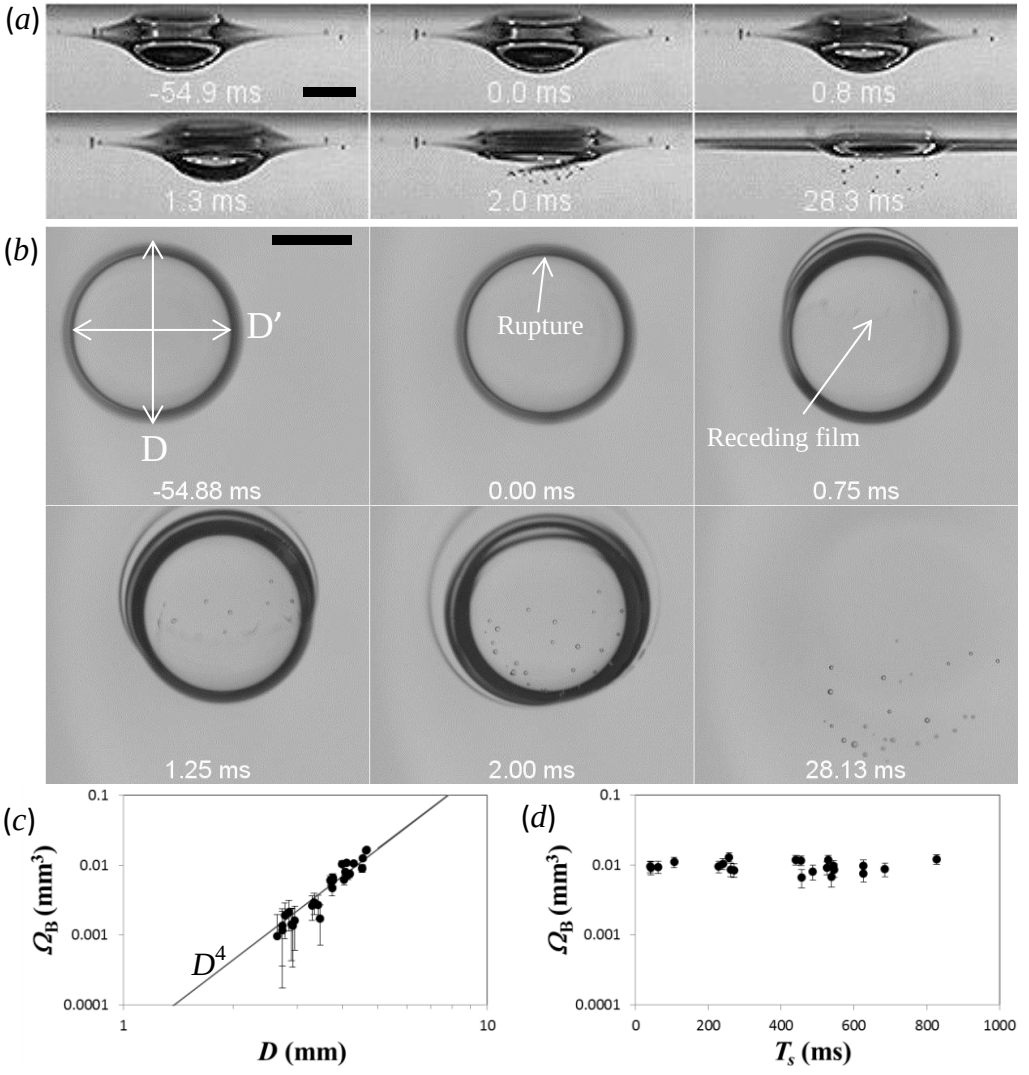

FIGURE 6. Droplet rupture. (a) Side view from just below the free surface and (b) bottom-up view of droplet coalescence. Rupture begins at $t_r = 0$ ms (second frame). Error in relative times between (a) and (b) is less than 0.05 ms. Scale bar is 2 mm. (c) Total bubble volume as a function of droplet diameter. N=33. (d) Total bubble volume as a function of droplet lifetime for $D = 4.1$ mm, with T_s measured from the onset of skirting ($t_s = 0$). N=22

slipping on a surface. For such a sphere, the function $x(\theta)$ is shown in figure 9c with $u_s = (1/2)u_D$. In the case of rolling without slipping, we would expect a slope of zero at $x(\theta = 3\pi/2)$ (inset of figure 9c). It is important to note that slipping in this case is with respect to the stationary lab frame. It is shown below that the surface of the bath just below the droplet also has a forward motion.

Upon impact excess pressure is built up in the air gap between the droplet and the bath. This has been discussed extensively in the literature (Jones & Wilson 1978), (Bouwhuis *et al.* 2012) for vertically impacting droplets. The oblique impact of the droplets in this work must also induce a higher pressure below the droplet. Because of the asymmetry of the impact, this excess pressure will impart a torque on the droplet and initiate rotation.

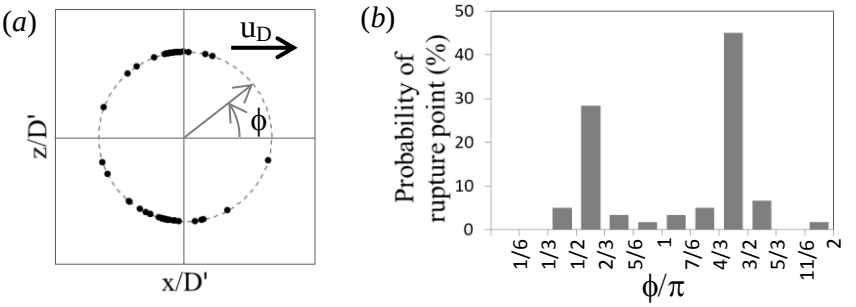

FIGURE 7. Angular distribution of rupture points. (*a*) Positions of rupture initiation relative to the boundary of the air gap. (*b*) Distribution of rupture events. Bin size is $\pi/6$ with ϕ measured relative to the direction of the center-of-mass motion of the droplet as shown in (*a*). N=60.

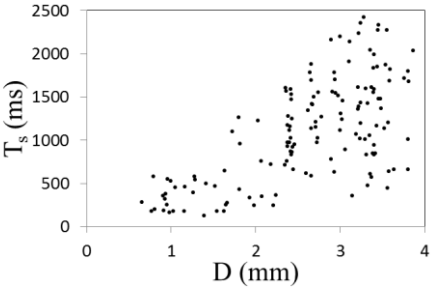

FIGURE 8. Droplet lifetimes, T_s as a function of droplet diameter.

For $t_s > 0$ the rate of rotation, measured by the droplet surface speed, u_s, decreases steadily. This is shown in figure 10*b* where u_s decreases slightly with respect to the center-of-mass speed of the droplet, u_D, which itself decreases exponentially in time (see figure 4). This indicates that the skirting motion cannot be the source of the rotation, since the rate of rotation would increase as the rolling motion of the droplet transitioned from slipping to no slipping.

The flow velocity in the bath, u_b, at the surface bounding the air gap also pointed forward as the droplet passed overhead (figure 10*b*), open circles and Movie 6)). For a 4.22-mm-diameter droplet u_b was approximately $u_D/2$. The relative speed of the bath surface, u_b/u_D, depends on droplet diameter as seen in figure 10*c*. When plotted against the Reynolds number both data sets collapse onto one line. For a 4.22 mm droplet, the velocity difference across the gap is approximately $u_D/5$ for early times and quickly approaches zero (figure 10*b*).

We can now return to the question above regarding the upwards lubrication force that delays droplet coalescence. We see now that the oblique impact imparts an angular momentum to the droplet, which in turn drives air into the gap at the leading edge. Because the air gap is more restricted on the trailing edge a lubrication force is supplied. Following Dell'Aversana *et al.* (1996), we can find a rough estimate of the size of this force using the known values of the measured parameters presented here. The simplest approximation is to assume the shape of the gap is that of an inclined plate with area A_g moving with relative speed Δu_g parallel to a stationary flat plate. In this case the normal force per unit width is (Batchelor 2010),

$$\frac{f_{\rm lub}}{W} = \frac{6\mu_{\rm air}\Delta u_g}{\alpha^2}\left\{\log\frac{h_1}{h_2} - 2\left(\frac{h_1-h_2}{h_1+h_2}\right)\right\}, \tag{3.4}$$

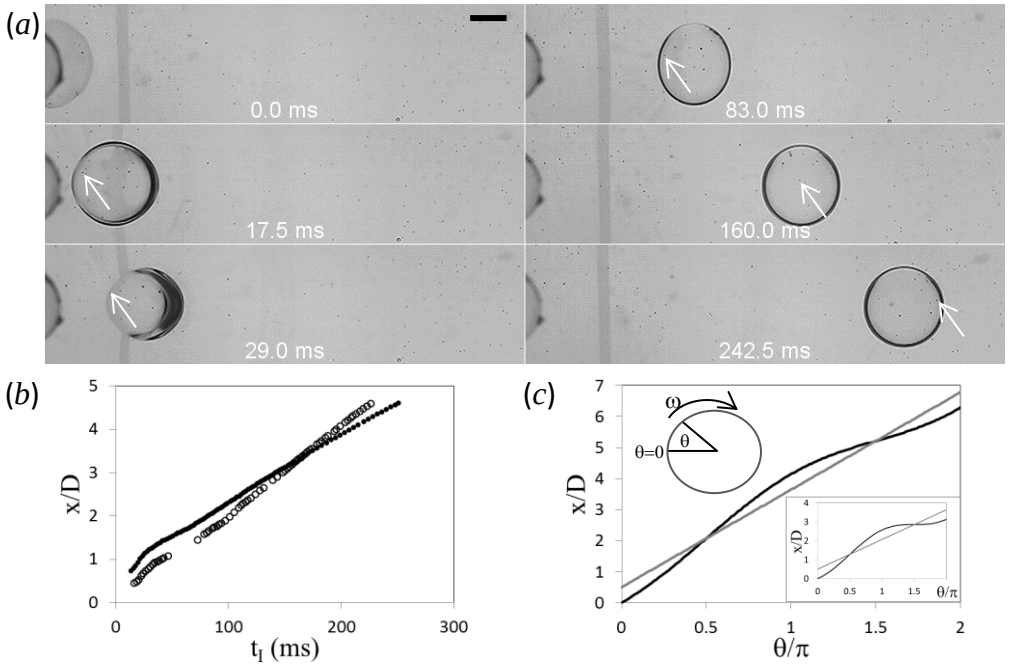

FIGURE 9. Initiation of droplet rotation. (a) Top view of initial impact and onset of rotation of a droplet. Arrow indicates a tracer particle that follows the surface of the droplet. Time is measured from impact; $t = t_I$. Scale bar is 2 mm. (b) Measured motion of the tracer particle indicated in (a) (closed circles) and the center-of-mass of the droplet (open circles). (c) Theoretical function $x(\theta)$ for a point on the surface of rotating sphere (black curve) with slipping (inset: without slipping), $\theta = 0$ is at the trailing edge of the sphere. Grey curve is the motion of the center-of-mass of the sphere.

where α is defined as the rate of change in the thickness going from the front ($h = h_1$) to the back ($h = h_2$) of the plate. For a linear gradient we can write α as $(h_1 - h_2)/D'$. If we consider the forces just prior to rupture, we can set $h_2 = 0.5\,\mu$m (near the range of van der Waals forces, $O(10^{-7})$ and $h_1 \sim \bar{h} = 1\,\mu$m. Then, using consistent values of D' and Δu_g from figure 10c, with $W = D'$ we find $f_{\text{lub}} = 3.1$ mN. The weight of the droplet is 0.4 mN. These values are only illustrative. Accurate values would require a model that better represents the true air gap profile measured through interferometry. In this simple model we see that the two forces are similar in magnitude, which can account for the delay in coalescence.

3.5. *Droplet deceleration*

We now turn our attention to the horizontal interactions that force the droplet to decelerate. To do so we investigated the fluid flow in the bath. Fluid flow at the surface of the bath is more complicated than flow in the droplet since it amounts to the superposition of wave motion with drag past a sphere. If we consider the moving dimple alone (somehow removing the droplet) a fluid particle under the surface of the bath would follow wave-like motion as illustrated in figure 11. The bath fluid in front of and behind the dimple ($t < t_2$ and $t > t_4$ in figure 11a) has a forward velocity whereas the bath fluid underneath the dimple ($t_2 < t < t_4$) flows opposite the velocity of the wave, giving rise to elliptical trajectories (figure 11b). The horizontal position versus time would be symmetrical and sinusoidal (inset to figure 11g).

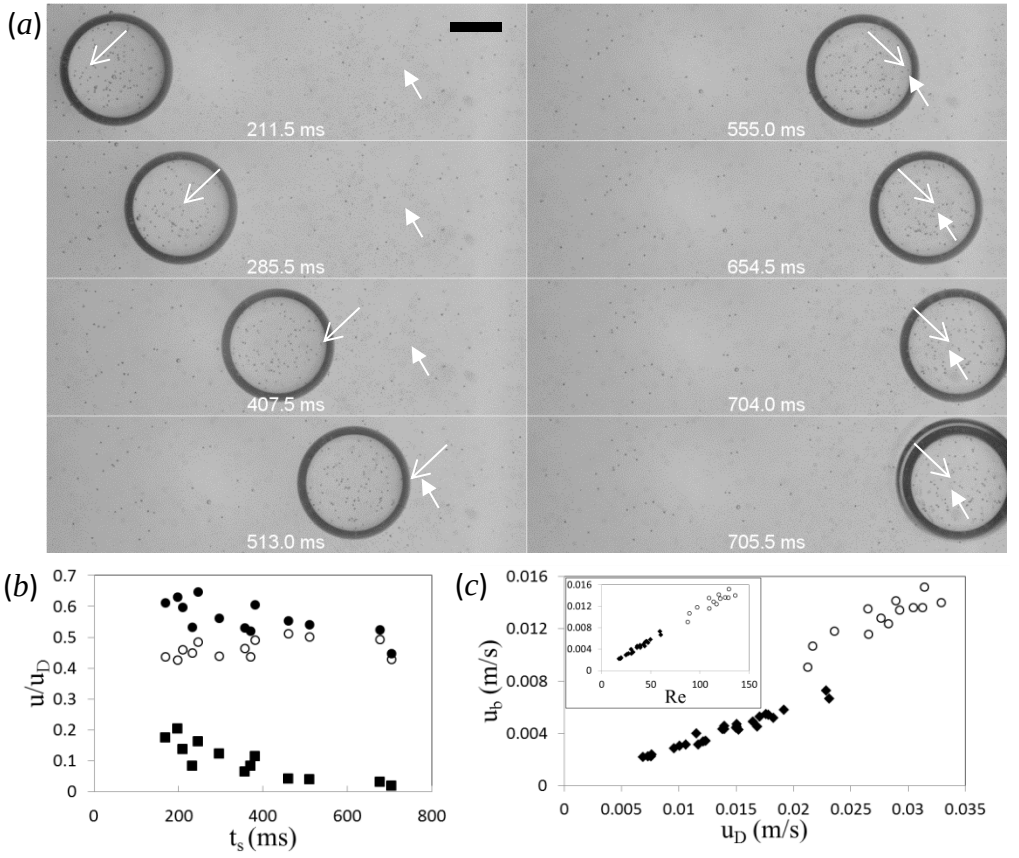

FIGURE 10. Droplet, droplet surface and bath surface speeds. (a) Bottom-up view of a skirting droplet. Polystyrene microbeads mark the rotation of a skirting droplet ($D = 4.22$ mm). A bead moving with the surface of the droplet (open arrow) travels forward with a speed greater than the center-of-mass speed of the droplet when along the top of the droplet ($t_s < 513.0$ ms). The same bead continues forward with a speed less than the center-of-mass speed of the droplet when along the bottom of the droplet ($t_s > 513.0$ ms). A glass bubble marks the fluid flow at the surface of the bath (closed arrow) and accelerates forward as the droplet passes over. Scale bar = 2 mm. (b) The droplet surface speed at the gap (u_s, closed circles) and the bath surface speed (u_b, open circles) along with their difference ($\Delta u_g = u_s - u_b$, squares) are plotted as a function of t_s. Each marker indicates a different droplet. N=13. (c) The bath surface speed for two different droplet sizes ($D = 4.22$ mm, open circles; $D = 2.66$ mm, closed diamonds). The same data is plotted against the Reynolds number (inset).

For the case at hand, that of a rolling droplet propelling the dimple forward, the viscous coupling between the droplet and the bath is evident by perturbations to the otherwise wave-like motion of the bath. In particular the bath is seen to move forward throughout the time the dimple passes by (figure 11c - g; also see Movie 6). Fluid at the surface that was near or underneath the droplet continued forward ($x(t)$ grows monotonically) throughout the motion of the droplet (figure 11d and open and closed squares of figure 11f & g). Further out from the air gap region the bath surface flow was less influenced by the viscous coupling leading to more wave-like behavior evidenced by closed trajectories (open circles in figure 11e) and a maximum in $x(t)$ (open circles in figure 11g).

During the skirting motion the Reynolds numbers decrease from $Re\,O(100)$ to $Re\,O(10)$ at coalescence when using the center-of-mass speed of the droplet as the characteristic

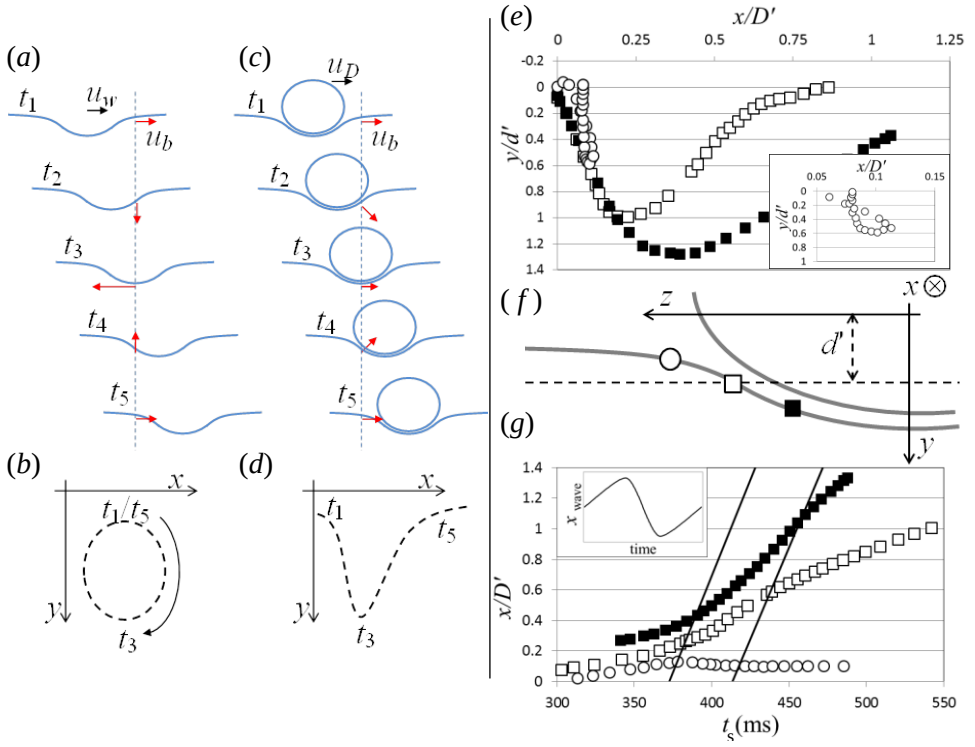

FIGURE 11. Free surface flow under a skirting drop. (a) A wave pulse with wave speed, u_w, and flow velocity at the dimple, u_b, gives rise to (b) closed elliptical paths, whereas (c) a skirting droplet (u_D is the velocity of the droplet/dimple system) forces the bath surface to be translated forward (d). (e) Trajectories of fluid markers at the surface of the bath (symbols explained in (f)). y and x are normalized by the air gap depth d' and air gap diameter D', respectively. Inset emphasizes the closed trajectory of a fluid marker near the edge of the droplet as illustrated in (f). (f) Schematic representation of the position of the fluid markers relative to the lowest point in the dimple. The droplet moves into the page (positive x direction). The bath surface fluid flows into the page but under (open and closed squares) or around (open circles) the droplet. (g) $x(t)$ for the three fluid markers increases monotonically for those that flow under the droplet (open and closed squares) but has a turning point for those that flow around the droplet (open circles). The two straight lines represent the position of the leading edge (t_2) and trailing edge (t_4) of the air gap boundary. Inset shows $x(t)$ expected for pure wave motion.

speed. Though these numbers are low they do not exclude inertial effects. However, the motion of the bath does indicate an absence of inertial forces. This is supported by two observations above. First, the component of the surface area bounding the air gap normal to the flow is large compared to the tangential component. Much like a two dimensional disk whose plane is parallel to the flow has no pressure forces, the pressure forces for the air gap geometry for skirting droplets are small. Second, the motion of the bath around the dimple is wave-like, with perturbations only below the air gap region. Though pressure forces certainly exist for this problem and are the cause of lift, the net force in the horizontal plane is dominated by viscous drag.

To begin modeling this problem we note that, according to reciprocity, the shear force at the surface of the bath acts to slow the droplet and to drag the bath forward with equal magnitude. Despite the velocity gradient across the air gap (as well as the velocity gradient from the droplet surface to its center-of-mass) we can calculate this force without a detailed knowledge of these gradients. Though this shear force also imparts a torque

on the droplet in a complex way, the center-of-mass acceleration of the droplet results from the net force acting on the droplet, irrespective of the position the force is applied. Further, the shear force at the surface of the bath acts on the air gap/droplet system, but the negligible mass of the entrained air will not affect the acceleration of the droplet.

The speed at the surface of the bath bounding the air gap is u_b. The shear force at the bath surface is equal to the Stokes flow drag on a fictitious rigid spheroidal cap moving at speed u_b with a no-slip condition. The Stokes drag on a fully submerged, solid sphere of diameter D and speed u moving through a surrounding medium with viscosity μ is,

$$f_{\mathrm{s}}^{*} = \frac{3\mu u_b}{D} A_{\mathrm{sphere}} = 3\pi\mu u_b D, \tag{3.5}$$

which results from a constant viscous term integrated over the area of the complete sphere (Batchelor 2010). The same is not true for a rigid oblate spheroid. However, for small deviations from a sphere (ϵ is small) the resulting drag is different only by a geometry dependent factor, β (Ramkissoon 1997),

$$f_{\mathrm{s,spheroid}} = \frac{3\mu u_b}{D} A_{\mathrm{spheroid}}\beta,\ \beta = \frac{2}{5}\left(2 + \frac{b}{D}\right). \tag{3.6}$$

Here the surface area of the spheroid, A_{spheroid}, is approximated to be the same as a sphere with diameter D. Flattening of the droplets is driven by a reduction of gravitational energy with an increase in surface energy until the two are balanced (Mahadevan & Pomeau 1999). It can be shown that for $Bo \approx 1$, which is the case for the range of droplet diameters explored in this work, β decreases approximately linearly with D (the derivation is given in the supplemental materials); larger droplets are more elliptical which leads to decreasing β. For larger flattening ($0 < \epsilon < 1$) the simple linear factor in equation 3.6 is no longer valid, though we expect β to continue decreasing with increasing D. Assuming this is the case for a spheroidal cap with area A_g and surface speed u_b, we write the Stokes drag as,

$$f_{\mathrm{s}} \propto \frac{\mu A_g}{D^2} u_b. \tag{3.7}$$

By Newton's Second Law, this force acts to decelerate the droplet:

$$f_{\mathrm{s}} = \rho\Omega_D \frac{du_D}{dt_s}. \tag{3.8}$$

Here ρ is the density of the droplet, Ω_D and u_D are the volume and center-of-mass speed of the droplet, and t_s is the time from the onset of skirting. The Stokes drag scales with the flow speed at the bath surface, u_b, whereas Newton's Second Law relates the net force to the change in the center-of-mass speed of the droplet, u_D. It is reasonable to suggest that u_b scales linearly with u_D. In fact u_b scales with the product $u_D D$ (see figure 10*c*). Replacing u_b with $u_D D$ in Equation 3.7 and combining Equations 3.7 and 3.8 we get, after some rearranging,

$$\frac{du_D}{u_D} = -\frac{dt_s}{\tau},\ \tau \propto \frac{2\Omega_D D}{3\nu A_g}, \tag{3.9}$$

with ν the kinematic viscosity and τ, measured here in milliseconds, representing a characteristic deceleration time. Integrating this twice we find $x(t)$ which can then be fit to the data,

$$x(t) = u_{D0}\tau\left(1 - e^{-t/\tau}\right). \tag{3.10}$$

Here, u_{D0} is the speed at $t_s = 0$. This result gives the expected motion observed for skirting droplets and confidently fits the data (figure 4*c*). Fitting each trajectory with

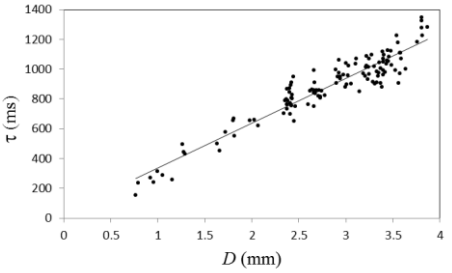

FIGURE 12. The rate of decay of velocity, τ, as a function of droplet diameter.

Equation 3.10 gives the value of the fit parameters u_{D0} and τ, which we now see is the decay constant of the observed exponential motion. Given that the volume of the asymmetric ellipsoidal droplet does grow as the expected D^3 and the air gap area scales as D^3, as shown earlier, equation 3.9 suggests that $\tau \propto D$ with both τ and D measurable. The data confirms this scaling law as seen in figure 12.

4. Conclusions

In this report we have presented the first quantitative description of droplets moving along the surface of a quiescent pool for which no driving force is supplied. Surfactant laden droplets can survive the violent impact in which significant deformations of the droplet and bath occur. After impact the droplets skirt along the surface quasi-statically with exponentially decreasing velocity until eventual coalescence. The droplet rolls with slipping in a wave-like dimple. The fluid motion in the bath in the vicinity of the dimple shows a viscous drag from the droplet on the bath through the thin air gap that separates the two. Despite Reynolds numbers too large to suggest a Stokes flow approximation, the geometry of the air gap and wave-like motion of the dimple allow such an assumption.

With the observation of bubbles forming at rupture, we have shown that an air gap does indeed separate the droplet from the bath. This air gap is thinnest at the inflection point of the bath dimple along the sides of the droplet transverse to the direction of motion. Though the detailed morphology of the air gap remains unknown, the total volume of air in the gap is constant throughout the motion. For driven systems the air gap is maintained in steady state. For stationary droplets the air gap thins similar to the Reynolds limit for approaching parallel disks (Amarouchene *et al.* 2001). For the case of skirting droplets the angular momentum imparted at impact acts to drive air into the gap, thus replenishing the gap and delaying coalescence.

We have also described the transient dynamics of the center-of-mass of the skirting droplets. In particular, owing to the flattening of the droplet (Bo is $O(1)$), the air gap area scales closer to the cube of the diameter rather than quadratically. This leads to an exponential deceleration with a decay time that scales linearly with droplet diameter. This is explained by a model of Stokes drag and is verified by the data.

The phenomenon presented here has been of interest for over a century and the topic of relative tangential motion between a droplet and a bath of the same fluid continues to garner interest (Alghoul *et al.* 2011), (Che *et al.* 2015). Skirting droplets can arise in industrial applications such as surface coatings or spray painting. Understanding the physics of droplet noncoalescence for such systems can lead to progress in applications that obey similar physics.

We would like to thank Melinda Franke and John Stanton for assistance in collecting rupture data and Hunter Klein and Andrew Merritt for assistance in collecting flow speed data. We would also like to thank Drew Rohm-Ensing for assistance with preliminary experiments. Additionally, we are grateful to the reviewers for helpful comments regarding both the content and presentation in the manuscript. This work was supported by funds from DePauw University.

REFERENCES

Alghoul, Samah K., Eastwick, Carol N. & Hann, David B. 2011 Normal droplet impact on horizontal moving films: an invesigation of impact behaviour and regimes. *Experiments in Fluids* **50**, 1305 – 1316.

Amarouchene, Y., Cristobal, G. & Kellay, H. 2001 Noncoalescing drops. *Physical Review Letters* **87** (20), 206104 (4).

Andersen, Anders, Madsen, Jacob, Reichelt, Christian, Ahl, Sonja Rosenlund, Lautrup, Benny, Ellegaard, Clive, Levinsen, Mogens T. & Bohr, Tomas 2015 Double-slit experiment with single wave-driven particles and its relation to quantum mechanics. *Physical Review E* **92**, 013006 (14).

Aryafar, H. & Kavehpour, H. P. 2008 Hydrodynamic instabilities of viscous coalescing droplets. *Physical Review E* **78**, 037302 (4).

Batchelor, G. K. 2010 *An introduction to fluid dynamics*, 14th edn. 32 Avenue of the Americas, New York, NY 100013-2473, USA: Cambridge University Press.

Bouwhuis, Wilco, van der Veen, Roeland C. A., Tran, Tuan, Keij, Diederik L., Winkels, Koen G., Peters, Ivo R., van der Meer, Devaraj, Sun, Chao, Snoeijer, Jacco H. & Lohse, Detlef 2012 Maximal air bubble entrainment at liquid-drop impact. *Physical Review Letters* **109**, 264501 (4).

Cai, Y. K. 1989 Phenomena of a liquid drop falling to a liquid surface. *Experiments in Fluids* **7**, 388 – 394.

Charles, G. E. & Mason, S. G. 1960*a* The coalescence of liquid drops with flat liquid/liquid interfaces. *Journal of Colloid Science* **15**, 236 – 267.

Charles, G. E. & Mason, S. G. 1960*b* The mechanism of partial coalescence of liquid drops at liquid/liquid interfaces. *Journal of Colloid Science* **15**, 105 – 122.

Che, Zhizhao, Deygas, Amandine & Matar, Omar K. 2015 Impact of droplets on inclined flowing liquid films. *Physical Review E* **92**, 023032 (13).

Ching, Bruce, Golay, Michael W. & Johnson, Thomas J. 1984 Droplet impacts upon liquid surfaces. *Science* **226** (4674), 535 – 537.

Couder, Yves & Fort, Emmanuel 2006 Single-particle diffraction and interference at a macroscopic scale. *Physical Review Letters* **97**, 154101 (4).

Couder, Y., Fort, E., Gautier, C.-H. & Boudaoud, A. 2005 From bouncing to floating: noncoalescence of drops on a fluid bath. *Physical Review Letters* **94**, 177801 (4).

Dell'Aversana, P., Banavar, J. R. & Koplik, J. 1996 Suppression of coalescence by shear and temperature gradients. *Physics of Fluids* **8** (1), 15 – 28.

Esmailizadeh, L. & Mesler, R. 1986 Bubble entrainment with drops. *Journal of Colloid and Interface Science* **110** (2), 561 – 574.

Fort, Emmanuel, Eddi, Antonin, Boudaoud, Arezki, Moukhtar, Julien & Couder, Yves 2010 Path-memory induced quantization of classical orbits. *Proceedings of the National Academy of Sciences* **107** (41), 17515 – 17520.

Gatne, Kalpak P., Jog, Milind A. & Manglik, Raj M. 2009 Surfactant-induced modification of low Weber number droplet impact dynamics. *Langmuir* **25** (14), 8122 – 8130.

Hahn, Phil-Soo, den Chen, Jing & Slattery, J. C. 1985 Effects of London-van der Waals forces on the thinning and rupture of a dimpled liquid film ans a small drop or bubble approaches a fluid-fluid interface. *AlChE Journal* **31** (12), 2026 – 2038.

Hendrix, Maurice H., Bouwhuis, Wilco, van der Meer, Devaraj, Lohse, Detlef & Snoeijer, Jacco H. 2016 Universal mechanism for air entrainment during liquid impact. *Journal of Fluid Mechanics* **789**, 708 – 725.

Honey, E. M. & Kavehpour, H. P. 2006 Astonishing life of a coalescing drop on a free surface. *Physical Review E* **73**, 027301 (4).

Hsiao, Mingying, Lichter, Seth & Quintero, Luis G. 1988 The critical Weber number for vortex and jet formation for drops impinging on a liquid pool. *Physics of Fluids* **31** (12), 3560 – 3562.

Jones, A. F. & Wilson, S. D. R. 1978 The film drainage problem in droplet coalescence. *Journal of Fluid Mechanics* **87**, 263 – 288.

Keller, Joseph B. 1998 Surface tension force on a partly submerged body. *Physics of Fluids* **10** (11), 3009 – 3010.

Klyuzhin, I. S., Ienna, F., Roeder, B., Wexler, A. & Pollack, G. H. 2010 Persisting water droplets on water surfaces. *Journal of Physics Chemistry B* **114**, 14020 – 14027.

Lhuissier, H., Tagawa, Y., Tran, T. & Sun, Chao 2013 Levitation of a drop over a moving surface. *Journal of Fluid Mechanics* **733**, R4 – (14).

Mahadevan, L. & Pomeau, Y. 1999 Rolling droplets. *Physics of Fluids* **11** (9), 2449 – 2453.

Mills, B. H., Saylor, J. R. & Testik, F. Y. 2011 An experimental study of Mesler entrainment on a surfactant-covered interface: the effect of drop shape and Weber number. *AlChE Journal* **58** (1), 46 – 58.

Neitzel, G. Paul & Dell'Aversana, Pasquale 2002 Noncoalescence and nonwetting behavior of liquids. *Annual Review of Fluid Mechanics* **34**, 267 – 289.

Ooi, Chin Hong, Vadivelu, Raja K., John, James St, Dao, Dzung Viet & Nguyen, Nam-Trung 2015 Deformation of a floating liquid marble. *Soft matter* **11**, 4576 – 4583.

Pirat, C., Lebon, L., Fruleux, A., Roche, J.-S. & Limat, L. 2010 Gyroscopic instability of a drop trapped inside an inclined circular hydraulic jump. *Physical Review Letters* **105**, 084503 – (4).

Ramkissoon, H. 1997 Slip flow past an approximate shperoid. *Acta Mechanical* **123**, 227 – 233.

Reynolds, Osborn 1881 On drops floating on the surface of water. *Chemical News* **44**, 211 – 212.

Saylor, John & Bounds, Garrett 2012 Experimental study of the role of the Weber and capillary numbers on Mesler entrainment. *AlChE Journal* **58** (12), 3841 – 3851.

Sreenivas, K. R., De, P. K. & Arakeri, Jaywant H. 1999 Levitation of a drop over a film flow. *Journal of Fluid Mechanics* **380**, 297 – 307.

Thoroddsen, S. T. & Takehara, K. 2000 The coalescence cascade of a drop. *Physics of Fluids* **12** (6), 1265 – 1267.

Tran, Tuan, de Maleprade, Helene, Sun, Chao & Lohse, Detlef 2013 Air entrainment during impact of droplets on liquid surfaces. *Journal of Fluid Mechanics* **726**, R3 (11).

Walker, J. 1978 Drops of liquid can be made to float on liquid. What enables them to do so? *Scientific American* **238** (6), 151 – 158.